Ultrasound compounding with automatic attenuation compensation using paired angle scans

G.M. Treece, R.W. Prager and A.H. Gee

CUED/F-INFENG/TR 558

June 2006

Cambridge University Engineering Department
Trumpington Street
Cambridge CB2 1PZ
England

Corresponding e-mail: gmt11@eng.cam.ac.uk

Abstract

Variations in attenuation in tissue can result in shadowing and enhancement in ultrasound images. Angular compounding of ultrasound images by lateral beam-steering can be used to improve delineation of structures, but causes such shadows and enhancements to appear in less recognisable forms. We present an algorithm which uses lateral beam-steering to produce compounded images with significantly reduced artefacts. This is compared to several other alternative algorithms for attenuation estimation, some of them embedded for the first time in a multi-angle framework. Algorithms are tested on simulated and *in vitro* data in 2D and 3D contexts. The new algorithm is as good as the best alternative on all data sets tested, and is straightforward to implement.

Contents

1 Introduction

Medical ultrasound images contain many artefacts due to the complex nature of sound transmission and reflection in anatomical structures. Shadowing and enhancement, for instance, are the result of variations in attenuation throughout the image. This can be compensated in the vertical direction by a set of time-gain sliders which control the gain in horizontal bands across the image. Gain variations in the horizontal direction remain, however, appearing as over-compensated bright patches under regions of low attenuation (enhancement) or under-compensated dark patches under regions of high attenuation (shadowing).

Since shadows and enhancements are in effect indicators of relative attenuation in over-lying regions, something which is otherwise not displayed, they can in some cases have clinical significance. For instance, this has been demonstrated in detecting liver disease (Bevan and Sherar, 2001) or certain tumours (Tu et al., 2003), or even for monitoring temperature change (Tyréus and Diederich, 2004). However, in other cases they can simply be confusing. This is particularly the case for 3D data, where the visualisation planes are not in general along the direction of insonification. In such planes, shadows or enhancements can appear without the corresponding anatomy which generated them.

In any case, it would seem logical to display attenuation effects separately from signal backscatter (or reflection) which is the main component of ultrasound images. Certainly this would ease the interpretation of ultrasound images, and make downstream processing (for instance segmentation) more reliable. The estimated attenuation can then be displayed as a separate image, rather than having to infer it from artefacts in an image essentially of ultrasound backscatter.

1.1 Attenuation estimation

One technique for reducing shadowing and enhancement is to attempt to estimate the attenuation independently from the backscatter. Having estimated the attenuation at all points in an image, it is straightforward to adjust the image for this known attenuation, therefore removing artefacts. Such approaches have been reviewed in a previous paper (Treece et al., 2005). All rely on certain assumptions regarding the ultrasound signals. The algorithm of Hughes and Duck (1997) deduces attenuation directly from the backscattered signal by assuming that the attenuation is directly proportional to the backscatter. Flax et al. (1983) assume that the ultrasound pulse has a broadly Gaussian spectrum, and use the shift in centre frequency to estimate attenuation. Knipp et al. (1997) compare the backscattered spectrum with a calibration spectrum to estimate attenuation. Both these last methods require the scattering spectrum of the sample to be the same as in a calibration object.

1.2 Angular compounding

Angular compounding, where the ultrasound beam is steered laterally to various angles and the resulting images averaged, was first proposed over twenty years ago (Berson et al., 1981), but has recently become more generally accessible (Entrekin et al., 1999, 2001; Jesperson et al., 1998). The main benefit of such compounding is to increase the signal to speckle ratio and reduce the dependency of reflection from planar interfaces on relative angle to the transducer. However, since shadowing and enhancements will always lie in the direction of insonification, angular compounding also has the subsidiary effect that these artefacts are blurred by the compounding procedure. Figure 5(a) and (b) show some *in vitro* examples — the strength of the shadow is not substantially reduced by compounding, but the appearance is somewhat different than in a conventional B-scan.

Several authors have recently attempted to use angular compounding on quantities other than signal magnitude, for instance attenuation (Tu et al., 2005), strain (Rao et al., 2006) and temperature (Pernot et al., 2004) estimates. In all cases, ultrasound scans at each insonification angle have simply been regarded as relatively independent estimates, which can be averaged to increase the information content. To our knowledge, the only paper which has investigated methods other than averaging from angular scans is by Wilhjelm et al. (2004), where various forms of median and maximum filters were investigated.

The novel approach in this paper is to use insonification from a variety of known angles to deduce the attenuation, rather than simply averaging results from each angle. It will be shown that, under certain assumptions, it is possible to calculate lateral variations in attenuation in a sample from the signal envelope of a pair of scans from equal and opposite steered angles. This information can be used to provide a compounded backscatter image free from shadows and enhancements. For comparison, we also embed the various competing attenuation estimation approaches in an angular compounding framework, in a similar manner to Tu et al. (2005).

We start in Section 2 by outlining a simple model for attenuation and backscatter, which allows us to develop the theory required for attenuation from paired-angle scans. We then outline various practical considerations necessary for implementing this theoretical result. In Section 3 the new algorithm is compared to other forms of attenuation correction, with and without compounding, using simulated and *in vitro* data. The results of these experiments are discussed in Section 4 and conclusions drawn in Section 5.

2 Method

2.1 Model for attenuation and backscatter

We deliberately adopt a simple model for the attenuation and backscatter in tissue. We assume that, at least over a small range of insonification angles, both the backscatter and attenuation from a particular location are isotropic. We further assume that the effect of attenuation on the centre frequency of the ultrasound pulse is small compared to the centre frequency. These two assumptions allow us to model the tissue with two scalar fields, $b(x, y)$ giving the backscatter coefficient in dB at (x, y) and $a(x, y)$ giving the attenuation coefficient in dB/cm at the average centre frequency of the ultrasound pulse in the tissue.

We also assume that the ultrasound pulse is everywhere perfectly focused and that the speed of sound is constant in the medium. Now the cumulative attenuation $c(x, y)$ from the pulse origin o to the scanned location (x, y) is simply twice the line integral of $a(x, y)$ along this path:

$$c(x, y) = 2 \int_o^{x,y} a(x, y) dr \tag{1}$$

where r represents distance along the insonification direction $\mathbf{r}$. The signal $v(x, y)$ (in dB) received at the transducer corresponding to the location (x, y) is now:

$$v(x, y) = b(x, y) - c(x, y) \tag{2}$$

Under these assumptions, a phantom with uniform background backscatter and attenuation and four inclusions themselves with different but nevertheless uniform backscatter and attenuation coefficients will generate a 'B-scan' as shown in Figure 1(a). The image is homogeneous and completely free of speckle, since the focusing is perfect and the underlying scattering is from a homogeneous material rather than from point scatterers, but it does contain shadowing and enhancement artifacts.

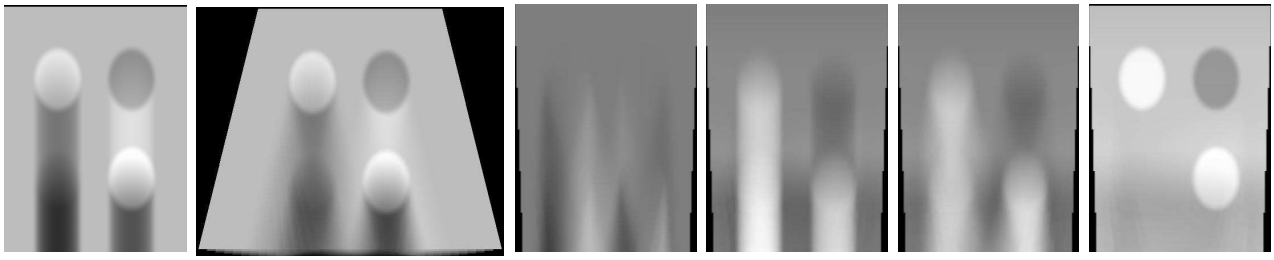

(a) (b) (c) (d) (e) (f)

Figure 1: **Attenuation correction in a simple tissue model.** (a) A 'B-scan' constructed from simple simulation data in which the backscatter and attenuation coefficients are modelled as scalar fields, and the focusing is ideal in all dimensions. Four spheres with varying backscatter and attenuation are embedded in a uniform background. (b) The result of conventional angular compounding applied to this model, using 15 angles varying from $-14°$ to $14°$ in steps of $2°$. (c) The average difference image between each pair of B-scans with equal and opposite angles. (d) The estimated cumulative attenuation for the $0°$ B-scan calculated from (c) using eq. (7). (e) The estimated cumulative attenuation for the compounded image in (b) using eq. (8). (f) The result of compensating (b) using (e) to eliminate shadowing and enhancement artifacts.

2.2 Derivation of paired angle compounding

We now consider a point (x, y) which is imaged from three different insonification directions at steering angles $-\theta°$, $0°$ and $\theta°$, as demonstrated in Figure 2. Although the received signal $v(x, y)$ is different in each case, in our model the underlying backscatter and attenuation coefficients in all three directions are the same. Since the attenuation at a point is the derivative of the cumulative attenuation along the direction of insonification, then comparing the two equal and opposite angle scans, we have:

$$a(x, y) = \nabla c_1(x, y) \cdot \hat{\mathbf{r_1}} = \nabla c_2(x, y) \cdot \hat{\mathbf{r_2}} \tag{3}$$

where the subscript 1 corresponds to an insonification angle of $-\theta°$ and 2 an insonification of $\theta°$. $\hat{\mathbf{r_1}}$ is a unit vector along the $-\theta°$ direction, and ∇ denotes the vector gradient operator.

We can substitute c in each case for b and v using eq. (2) (and remembering that, although c and v vary with insonification direction, b is constant across all directions, and hence needs no subscript):

$$\nabla \left(b(x, y) - v_1(x, y)\right) \cdot \hat{\mathbf{r_1}} = \nabla \left(b(x, y) - v_2(x, y)\right) \cdot \hat{\mathbf{r_2}} \tag{4}$$

Rearranging, and noting that $\hat{\mathbf{r_1}} = (\sin\theta, -\cos\theta)$ and $\hat{\mathbf{r_2}} = (-\sin\theta, -\cos\theta)$, we have:

$$\nabla b(x, y) \cdot \mathbf{i} = \frac{1}{2}\nabla \left(v_2(x, y) + v_1(x, y)\right) \cdot \mathbf{i} + \frac{1}{2\tan\theta}\nabla \left(v_2(x, y) - v_1(x, y)\right) \cdot \mathbf{j} \tag{5}$$

where $\mathbf{i}$ and $\mathbf{j}$ are unit vectors in the x and y directions respectively. Now integrating in the x direction, we have:

$$b(x, y) = \frac{1}{2}\left(v_2(x, y) + v_1(x, y)\right) + \frac{1}{2\tan\theta}\int_0^x \left[\nabla \left(v_2(x, y) - v_1(x, y)\right) \cdot \mathbf{j}\right] dx + K(y) \tag{6}$$

Note that since we have integrated in x, we are left with a function of y, $K(y)$ which we are unable to determine.

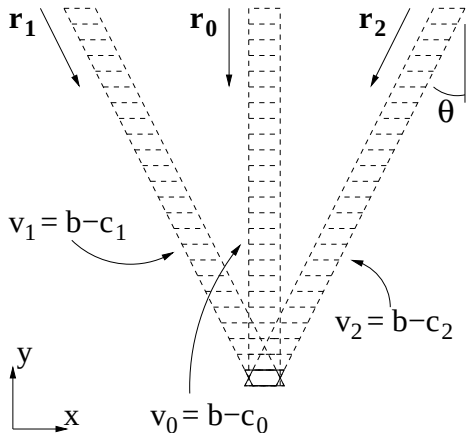

Figure 2: **Coordinate system for paired angle compounding.** Three ultrasound vectors are shown, at steering angles of $-\theta°$, $0°$ and $\theta°$. The vectors are in directions $\mathbf{r_1}$, $\mathbf{r_0}$ and $\mathbf{r_2}$ respectively. The underlying backscatter field is modelled as $b(x, y)$ and the attenuation field as $a(x, y)$. The cumulative attenuation $c_0(x, y)$ is formed by the line integral of $a(x, y)$ along $\mathbf{r_0}$, and similarly for $c_1(x, y)$ and $c_2(x, y)$, along $\mathbf{r_1}$ and $\mathbf{r_2}$ respectively. The received signal v_0 at an apparent location (x, y) is therefore equal to the backscatter at that location $b(x, y)$ minus the accumulated attenuation along $\mathbf{r_0}$ up to that point, $c_0(x, y)$.

It is also possible to find expressions for the cumulative attenuation in the $0°$ direction, by substituting b in eq. (6) using $c_0 = b - v_0$ from eq. (2):

$$c_0(x, y) = \frac{1}{2}\left(v_2(x, y) + v_1(x, y) - v_0(x, y)\right) + \frac{1}{2\tan\theta}\int_0^x \left[\nabla\left(v_2(x, y) - v_1(x, y)\right) \cdot \mathbf{j}\right] dx + K(y) \quad (7)$$

A similar substitution for $c_1(x, y)$ and $c_2(x, y)$ gives compounded cumulative attenuation $c_{comp}(x, y) = \frac{1}{2}\left(c_1(x, y) + c_2(x, y)\right)$, i.e. that which would need to be added to a compounded B-scan, as calculated from $\frac{1}{2}\left(v_1(x, y) + v_2(x, y)\right)$, to give a compounded backscatter image:

$$c_{comp}(x, y) = \frac{1}{2\tan\theta}\int_0^x \left[\nabla\left(v_2(x, y) - v_1(x, y)\right) \cdot \mathbf{j}\right] dx + K(y) \quad (8)$$

We can therefore create a compounded image free from attenuation artefacts by displaying $b(x, y)$, as defined in eq. (6). The first part of this equation is simply the average recorded signal v from multiple angles — i.e. a conventional compounded image. The second is our estimate of compounded attenuation, c_{comp}.

Figure 1 contains images of these scalar fields for a simulated phantom with four inclusions, some with larger and some with smaller values of a and b from the background (the bottom left inclusion has the same backscatter as the background, but higher attenuation). 127 RF signals were simulated at each of 15 steering angles, using a notional centre frequency of 10MHz, with amplitude v calculated using eq. (2) and perfect focusing in all dimensions. The signals were sampled at 66MHz with approximately 11 bits of signal resolution, in order to match our actual research ultrasound system.

2.3 Practical considerations

The main benefit of angular compounding is the increased delineation of structures due to the reduction in speckle from averaging over non-correlated images. It is important that this detail in the compounded image is preserved in any attempt to restore shadowed or enhanced regions. The conventional compounded image derives from the initial terms in eq. (6), and our estimate of attenuation from the later terms comprising c_{comp}, eq. (8). Hence, we must ensure that c_{comp} varies sufficiently smoothly such that the fine detail in the corrected compound image is relatively unaffected by the correction.

It can be seen from eq (8) that the cumulative attenuation is formed from the gradient in the j direction of the difference image between the B-scans. In practice, this gradient is small, particularly compared to the noise in this difference image due to variations in the actual speckle patterns and speed of sound, so we need a very robust estimator for this gradient. It is therefore estimated by a least squares fit of a line to a subset of the data centred about the point of interest. Typically this subset of data needs to be large, say 10 to 20 percent of the height of the image. However, we can dramatically increase the speed of this gradient operator by noting that we require a gradient estimate at every pixel in the image. In this context, it is far quicker to accumulate the required terms for the least squares estimation (e.g. $\sum x$, $\sum x^2$, etc.) over the entire height of the image. Then we simply take the difference between the accumulated estimates at each end of the window currently under consideration. This makes the computation time for the operation completely independent of the size of the least squares estimation window.

Angular compounding is usually performed over more than two angles. We can combine estimates for b from multiple pairs of angles by taking the weighted average of the difference images before we calculate the gradient, hence:

$$c_{comp}(x,y) = \int_0^x \left[\nabla \sum^{\text{paired angles}} \left[\frac{1}{2\tan\theta} \left(v_2(x,y) - v_1(x,y) \right) \right] \cdot \mathbf{j} \right] dx + K(y) \tag{9}$$

and the first term on the right hand side of eq. (6) then involves a sum over all the angles involved.

The calculations in eq. (6) are all performed in the same (x, y) coordinate system: the ultrasound signals v_1 and v_2, however, are not aligned with this system. We therefore need to interpolate them before proceeding. For convenience, we choose a grid of ultrasound vectors (in x) by display height in pixels (in y), aligned with the 0° signals v_0. We use vectors rather than the (generally smaller) pixels for the x direction, since this represents the true sampling resolution. We can afford to use display height rather than the much greater RF samples for the y direction, since we need many pixels for each gradient estimate, so the additional resolution from using samples is not required. Once we have an estimate for b, it is linearly interpolated in x to the display width in pixels in order to correct the aspect ratio before displaying.

Finally, it has already been noted that eq. (6) contains an unknown set of constants $K(y)$, i.e. we are not able to estimate the absolute gain of each horizontal row in the final image. Interestingly, this is precisely the function which is provided by the time-gain controls on an ultrasound machine. Eq. (6) therefore only models the variation in attenuation in the horizontal direction, which is all that is required to correct shadows and enhancements in the ultrasound data.

Nevertheless, we need to set $K(y)$ to some sensible value. We choose to set $K(y)$ such that the mean value of $c_{comp}(x, y)$ in eq. (8) over all y is zero. In practice, this sets the mean brightness of each row in the paired angle compounded image to the same as it would be in the conventional compounded image. Obviously if the algorithm were running live, this could be modified manually using the time gain control in the normal way.

Table 1: **Processing time.** The table shows frame rates (in frames per second) for each algorithm, including real-time data acquisition and display. The software was running on a 3.4GHz Intel PC with a Windows XP operating system.

Visualisation technique								
BSCAN		**SCATTER**		**CENTRE_FREQ**		**SPEC_DIV**		**PAIRED**
0°	comp	0°	comp	0°	comp	0°	comp	comp
35.3	2.4	12	0.8	5.5	0.4	5.0	0.3	2.0

Another consequence of $K(y)$ is that we cannot use this method to display the attenuation coefficient a directly[1]. Eq. (1) shows that this could be calculated from c_0 by taking the derivative in y, however this would include the derivative of $K(y)$, which we do not know.

3 Experiments and results

The algorithm was tested on simulation data and two different ultrasound phantoms. In all cases, compounding was performed by steering the ultrasound beam to 15 angles varying from $-14°$ to $14°$ in steps of $2°$. Ultrasound visualisations were generated by one of five methods:

BSCAN The conventional B-scan display of received amplitude.

SCATTER Attenuation correction using the method of Hughes and Duck (1997) in which the attenuation is assumed to be everywhere proportional to the backscatter.

CENTRE_FREQ Attenuation correction based on measuring the shift in centre frequency of the ultrasound pulse (Flax et al., 1983), using the method outlined in (Treece et al., 2005).

SPEC_DIV Attenuation correction using spectral division (Knipp et al., 1997) as outlined in (Treece et al., 2005).

PAIRED Attenuation correction using comparison of paired angle scans, as described in Section 2.

All methods were tested with and without angular compounding, save for PAIRED, which clearly cannot be used without angular compounding, since it is based on pairs of steered angle scans.

All algorithms were implemented in Stradwin[2] software for the acquisition and visualisation of 3D ultrasound data. This software can also be used to acquire real time RF ultrasound data from a Dynamic Imaging Diasus[3] ultrasound machine. Analogue RF data is digitised after focusing and time-gain compensation, but before log-compression and envelope detection, using a Gage Compuscope CS14200[4] 14-bit digitiser. Whole frames are stored in on-board Gage memory, before transferring to PC memory at 75 Mb/s. On average 30-60 frames can be acquired per second.

[1] We can, however, display an image of a where the mean at each y has been set to zero, which is perfectly adequate for revealing the location of attenuation variations, if not their actual values

[2] http://mi.eng.cam.ac.uk/~rwp/stradwin

[3] http://www.dynamicimaging.co.uk

[4] http://www.gage-applied.com

The Fourier Transforms required for CENTRE_FREQ and SPEC_DIV were implemented using the FFTW library[5] of Frigo and Johnson (1998). All algorithms were optimised to a similar degree: Table 1 shows typical frame rates for each method. Note that all the frame rates for compounding techniques would be increased if fewer than 15 angles were used, as is often the case.

The algorithms were tested on a variety of simulated and *in vitro* data, each with varying degrees of adherence to the assumptions outlined in the previous section. The simulated data had isotropic backscatter and attenuation and a constant speed of sound, but nevertheless modelled the actual blurring due to the various point spread functions at different steering angles. The attenuation phantom had notionally similar properties to the simulated data but with fairly weak shadowing and enhancement more typical of normal human tissue. The olive phantom was slightly more representative of *in vivo* conditions in that neither the speed of sound nor the scattering nor attenuation properties were controlled, although it is likely that the scattering was dominated by point scatterers and hence fairly isotropic. In addition, the contrast of attenuation between the olive and background was larger than in the attenuation phantom.

The performance of the algorithms in reducing shadowing and enhancement was tested by assessing the horizontal signal variation in regions containing shadows or enhancements over otherwise homogeneous material. B-scans were first median filtered at an appropriate level to remove the signal variation due to speckle. Then the standard deviation of the filtered signal in the lateral direction was calculated in dB, and this was used as a measure of the strength of the shadow or enhancement.

3.1 Field II simulations

Ultrasound simulations of spherical inclusions were calculated using Field II[6] (Jensen, 1996). The probe parameters were chosen to mimic the Dynamic Imaging Diasus 8-16 MHz linear array probe, which has a centre frequency of 10.5 MHz. Particular attention was paid to accurate modelling of the transmit and receive delays and apodization at each of the steering angles. Since these are programmed digitally in the Diasus, precisely the same values could be used in the simulation as in the real ultrasound machine. Four phantoms were modelled, shown in Figure 3, as follows:

Large +10 dB A cylindrical inclusion of diameter equal to half the probe width, backscatter 10 dB greater than background and attenuation 1.0 dB/cm/MHz greater than background.

Large -10 dB A cylindrical inclusion of diameter equal to half the probe width, backscatter 10 dB lower than background and attenuation 0.7 dB/cm/MHz lower than background.

Large 0 dB A cylindrical inclusion of diameter equal to half the probe width, backscatter the same as the background and attenuation 1.0 dB/cm/MHz greater than background.

Small various Four cylindrical inclusions of diameter equal to one quarter the probe width, backscatter varying from 10 dB less to 10 dB greater than background and attenuation varying from 1.0 dB/cm/MHz greater to 0.7 dB/cm/MHz less than background.

Modifications to these phantoms in order to simulate varying attenuation in Field II are described in Appendix A.

Figure 3 shows results for BSCAN (with and without compounding) and PAIRED algorithms. As expected, the compounded B-scan shows considerably better definition and reduced speckle when compared to the conventional B-scan. In addition, the shadow or enhancement in the compounded

[5] http://www.fftw.org

[6] http://www.es.oersted.dtu.dk/staff/jaj/field/

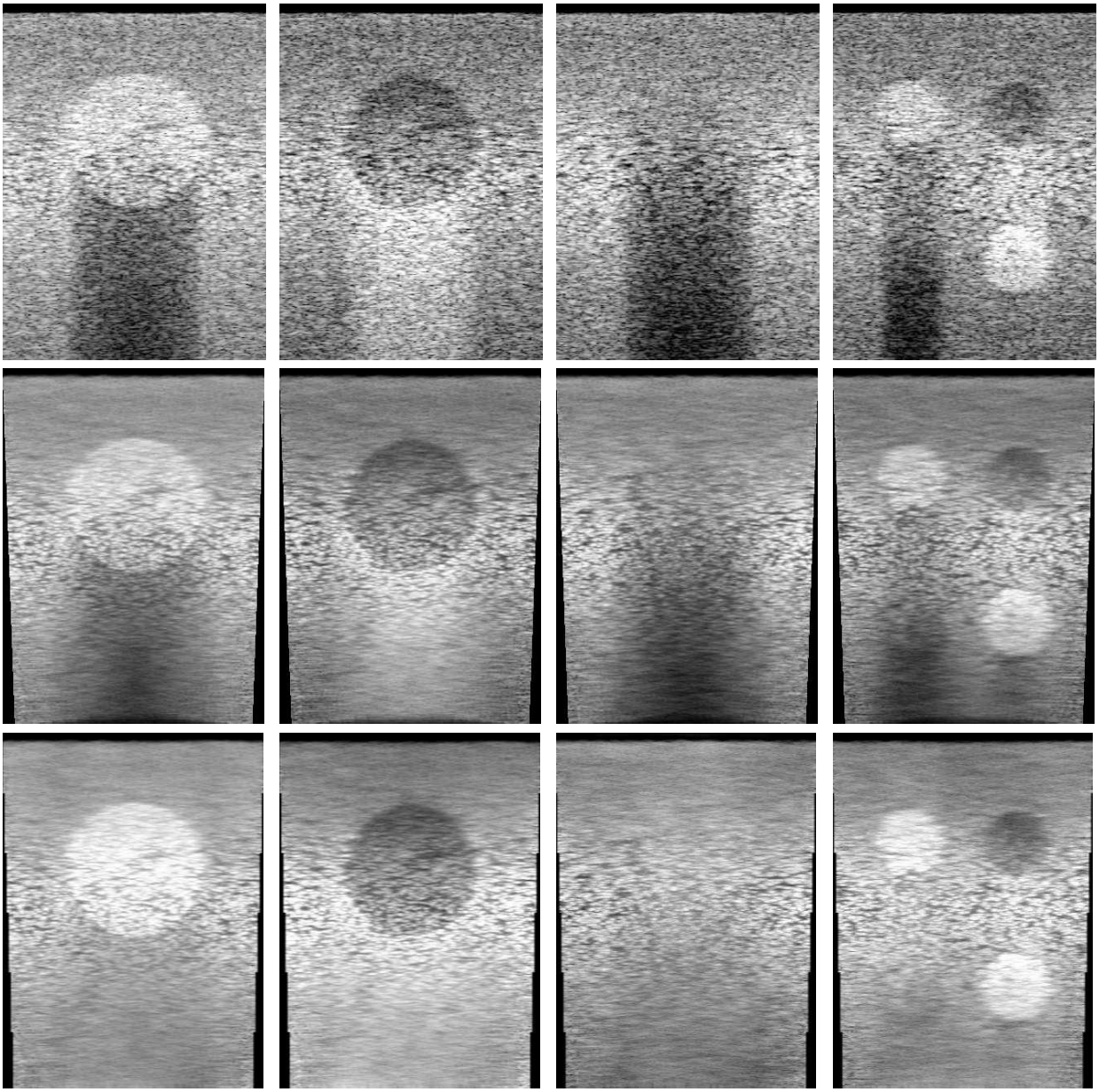

(a) (b) (c) (d)

Figure 3: **Simulations using Field II.** (a) A cylindrical inclusion with +10 dB backscatter and +1.0 dB/cm/MHz attenuation. (b) The same size cylinder with -10 dB backscatter and -0.7 dB/cm/MHz attenuation. (c) A cylinder with the same backscatter as the background, but +1.0 dB/cm/MHz attenuation. (d) Four smaller cylinders with varying backscatter and attenuation. In each case, the top row shows a B-scan, the middle row shows a conventional angular compounded B-scan, and the bottom row a B-scan compounded using the PAIRED algorithm.

Table 2: **Results for the Field II simulation.** The table shows the standard deviation of the brightness of the ultrasound image in the lateral direction, in dB measured over an area of homogeneous material, after median filtering to reduce speckle. A value of 0 indicates that the shadows or enhancements have been completely eliminated, larger values correspond to stronger shadowing or enhancement.

	Visualisation technique		
	BSCAN	**COMPOUNDED**	**PAIRED**
Large +10dB	11.50	8.96	1.86
Large -10dB	7.13	5.47	1.17
Large 0dB	10.55	8.34	1.99
Small various	8.09	6.18	2.12

image is reduced from a well delineated 'pillar' in the B-scan to a softer edged 'comet tail' in the compounded image. The PAIRED algorithm reduces the shadows and enhancements to a level where they are not immediately obvious in the images. Note that the PAIRED algorithm can only generate data in regions where two of the steered images overlapped. Conventional compounded images can generate data at more extreme angles, although data in these locations is less compounded than in the centre of the image. We have restricted the compounding region in this Figure to areas which have been covered by at least half the possible steering angles.

Table 2 contains numerical results for the Field simulations. Although conventional compounding does lower the strength of the shadow and enhancements a little, the reduction is not dramatic: the main effect is to alter the *shape* of these artefacts. The PAIRED algorithm, on the other hand, reduces the brightness variations to 2 dB or less in all cases, thus very nearly eliminating these artefacts completely. The simulation with four cylindrical inclusions demonstrates that the technique works equally well on data with a fairly complex attenuation field.

3.2 *In vitro* experiments

Both the CENTRE_FREQ and SPEC_DIV methods require a calibration scan of a homogeneous phantom, in order to account for time-gain control settings and focusing effects. This calibration scan was performed on a phantom with Rayleigh backscatter and a uniform attenuation of 0.55 dB/cm/MHz (J. M. Kofler and Madsen, 2001). The calibration spectra were then adjusted for the known attenuation in the phantom, as outlined in (Treece et al., 2005).

3.2.1 Attenuation phantom

An attenuation phantom was manufactured with varying spherical inclusions of known backscatter and attenuation[7] (J. M. Kofler and Madsen, 2001). The inclusions and background were manufactured with various densities of the same material containing small scale scatterers with a particular distribution of sizes, except for the -17 dB inclusions, which were manufactured from a different material containing small scale scatterers with a different distribution of sizes. The backscatter and

[7]E.L. Madsen, Department of Medical Physics, University of Wisconsin, 1530 Medical Science Centre, 1300 University Avenue, Madison, WI 53706-1532

Table 3: **Attenuation phantom properties.** The table shows the backscatter and attenuation coefficients for the attenuation phantom, all measured at 22°C and 10MHz.

Component	Backscatter (cf background) dB	Attenuation dB/cm/MHz	Attenuation (cf background) dB/cm/MHz
background	0	0.48	0
-17 dB spheres	-17	0.27	-0.21
+16 dB spheres	16	1.32	0.84
+8 dB spheres	8	0.70	0.22

Table 4: **Results for the attenuation phantom.** The table shows the standard deviation of the brightness of the ultrasound image in the lateral direction, in dB measured over an area of homogeneous material, after median filtering to reduce speckle. The 0° columns contain the non-compounded results, and 'comp' the compounded results.

	Visualisation technique								
	BSCAN		**SCATTER**		**CENTRE_FREQ**		**SPEC_DIV**		**PAIRED**
	0°	comp	0°	comp	0°	comp	0°	comp	comp
1.5 cm -17 dB	4.32	3.06	2.39	1.53	5.92	4.07	3.59	2.46	1.59
1.5 cm +16 dB	3.44	3.27	5.15	3.54	2.35	1.64	2.51	1.96	2.48
1.0 cm -17 dB	4.07	3.04	1.42	1.19	5.10	4.10	3.05	2.29	2.17
1.0 cm +16 dB	3.67	3.62	4.97	3.41	2.50	1.95	2.23	1.84	2.47
0.5 cm various	3.69	3.16	2.71	2.54	5.85	4.53	3.40	2.67	2.12

attenuation values are given in Table 3, chosen to reflect the expected variation in physiological tissue. The phantom included spheres of 1.5 cm, 1.0 cm and 0.5 cm diameter, in order to test the resolution of the algorithms.

Figure 4 shows sample results for the attenuation phantom, using all of the possible visualisation algorithms. In this case, the compounded images (other than PAIRED) are displayed at the full angular range in order to show the extent and quality of data available with each technique. As a result, the compounding varies from 15 scans at the centre of the images to only 1 scan (no compounding) at the edges. The shadows and enhancements are less obvious than in the Field simulation, but can still be clearly seen. From this figure it is clear that the SCATTER, SPEC_DIV and PAIRED algorithms all work well at reducing the attenuation artefacts.

The numerical results for this phantom in Table 4 clarify this point: in fact SCATTER works well for the -17 dB inclusions but not so well for the +16 dB ones. In contrast, CENTRE_FREQ works well for the +16 dB inclusions but not so well for the -17 dB ones. Only SPEC_DIV and PAIRED work well in all situations.

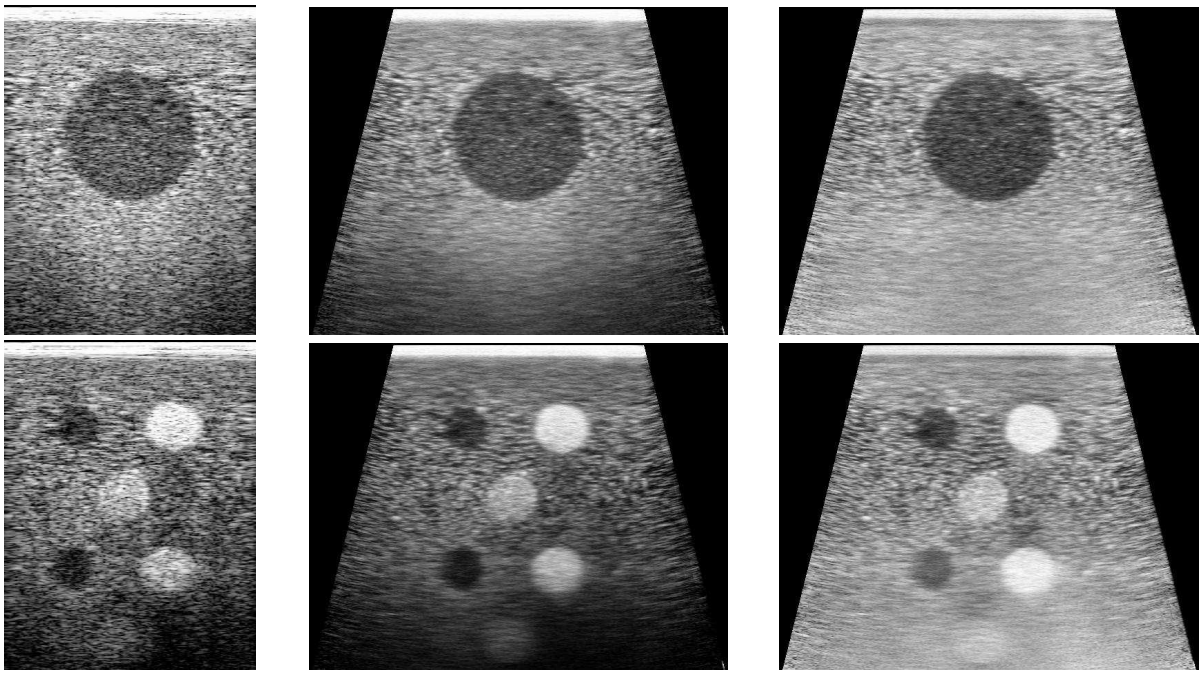

(a) BSCAN (b) COMPOUNDED (c) SCATTER

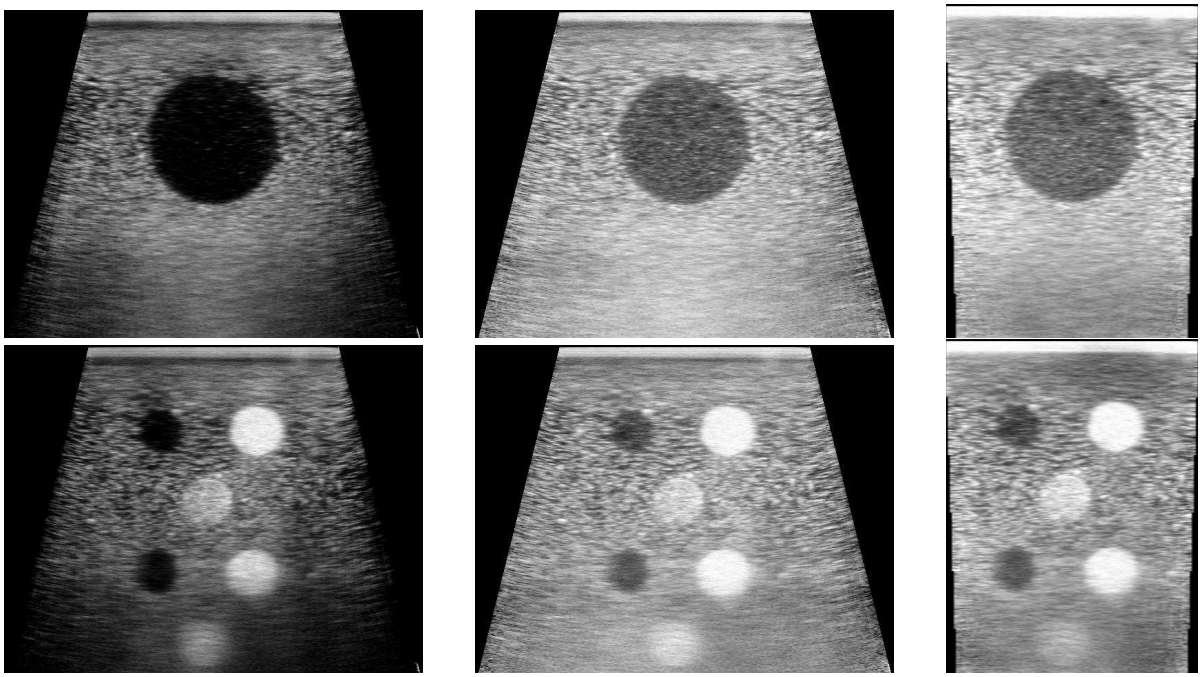

(d) CENTRE_FREQ (e) SPEC_DIV (f) PAIRED

Figure 4: **Attenuation phantom.** The top row shows the 1.5 cm -17 dB sphere, and the lower row the various 0.5 cm spheres in an attenuation phantom. (a) B-scan, (b) conventional angular compounding, (c) attenuation correction using SCATTER, (d) correction using CENTRE_FREQ, (e) correction using SPEC_DIV and (f) using PAIRED.

Table 5: **Results for the olive in jelly.** The table shows the standard deviation of the brightness of the ultrasound image in the lateral direction, in dB measured over an area of homogeneous material, after median filtering to reduce speckle. The 0° columns contain the non-compounded results, and 'comp' the compounded results.

	Visualisation technique								
	BSCAN		**SCATTER**		**CENTRE_FREQ**		**SPEC_DIV**		**PAIRED**
	0°	comp	0°	comp	0°	comp	0°	comp	comp
Longitudinal	19.45	15.88	4.92	3.59	6.44	9.00	5.57	7.04	4.39
Transverse	16.84	13.84	5.31	4.00	5.00	5.22	3.85	5.01	4.71

3.2.2 Olive in jelly

To provide a less controlled phantom (and hence with more of the characteristics of *in vivo* data), an olive was set in gelatin mixed with a small quantity of flour to provide some scatterers. This phantom contained some coherent reflection and was generally less homogeneous than the attenuation phantom. In addition, the olive was a stronger attenuator than the spherical inclusions in the attenuation phantom, and hence cast more obvious shadows.

Figure 5 shows typical scans of the olive phantom, both longitudinal and transverse. The transverse scan includes the centre of the olive, which was stuffed with pimento. Both the SCATTER and PAIRED algorithms work well with this phantom, SCATTER resulting in a slight residual enhancement, and PAIRED in a slight residual shadow. CENTRE_FREQ and SPEC_DIV are less impressive on this data.

Table 5 reveals that in this case CENTRE_FREQ and SPEC_DIV work better without angular compounding than with. Once again, the PAIRED algorithm results in reliable improvements to the attenuation artefacts in all cases.

3.3 3D scans

An olive phantom similar to that described in the previous section, but using a half olive rather than a stuffed olive, was scanned with a 10MHz wide band linear volume probe[8]. This probe was interfaced to the Dynamic Imaging Diasus system and to our Stradwin software such that we could control the beam-steering and the exact motion of the stepper motor driving the linear array. We were therefore able to acquire and visualise 3D angular compounded data.

Shadowing and enhancement artefacts are particularly problematic in 3D data, since visualisations out of the original B-scan planes do not reveal the source of these artefacts. Figure 6 shows some representative data from a scan of this olive phantom. The PAIRED algorithm clearly increases the contrast of the olive against the background and reduces the contrast of the shadow through the gelatin under the olive.

[8]RSP6-12, GE Healthcare, http://www.gehealthcare.com/usen/ultrasound/genimg/products/voluson730/vol730exp_probes.html

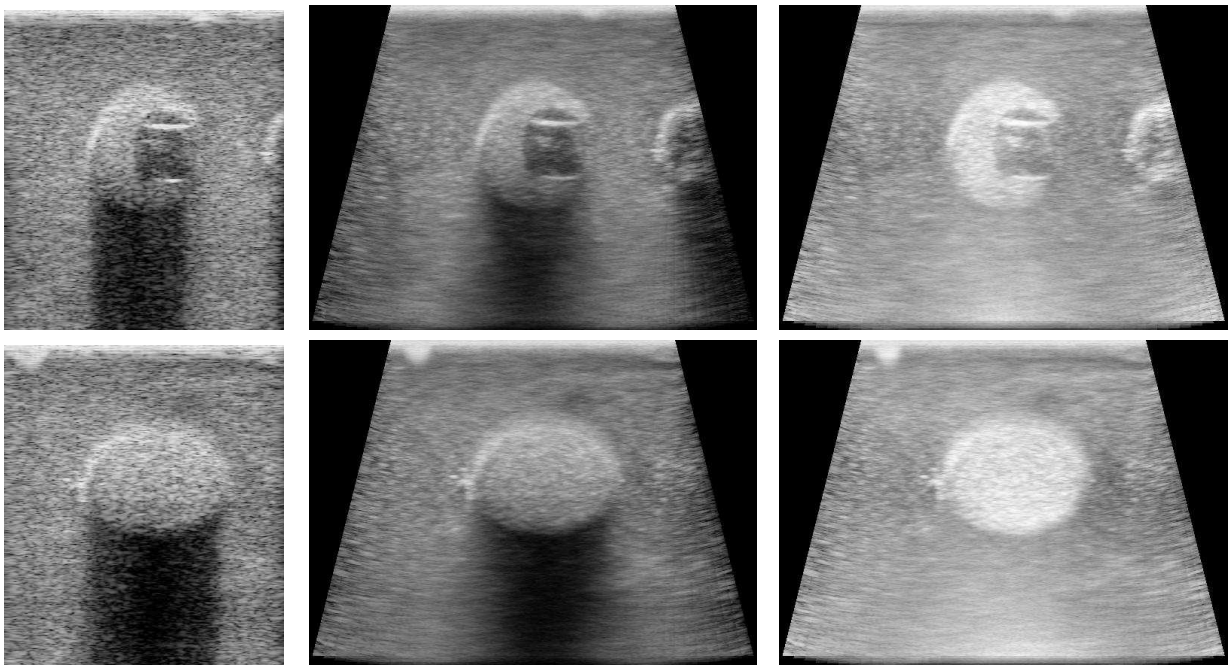

(a) BSCAN (b) COMPOUNDED (c) SCATTER

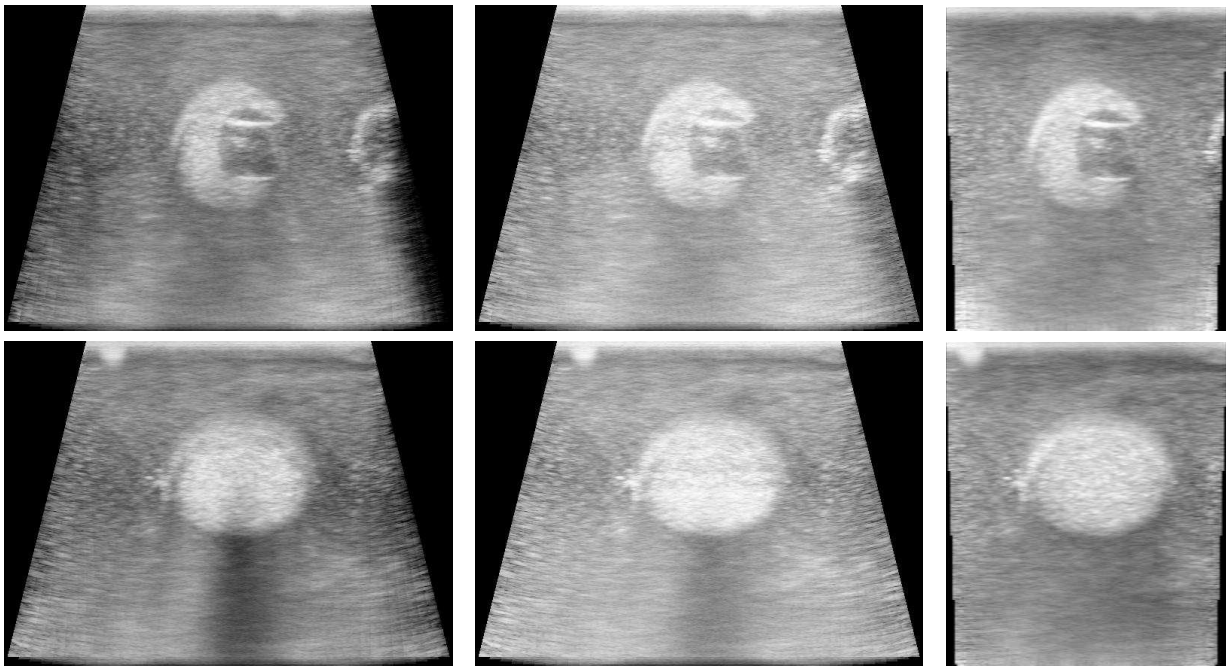

(d) CENTRE_FREQ (e) SPEC_DIV (f) PAIRED

Figure 5: **Olive phantom.** The top row shows a transverse, and the lower a longitudinal scan of an olive embedded in jelly mixed with flour. (a) B-scan, (b) conventional angular compounding, (c) attenuation correction using SCATTER, (d) correction using CENTRE_FREQ, (e) correction using SPEC_DIV and (f) using PAIRED.

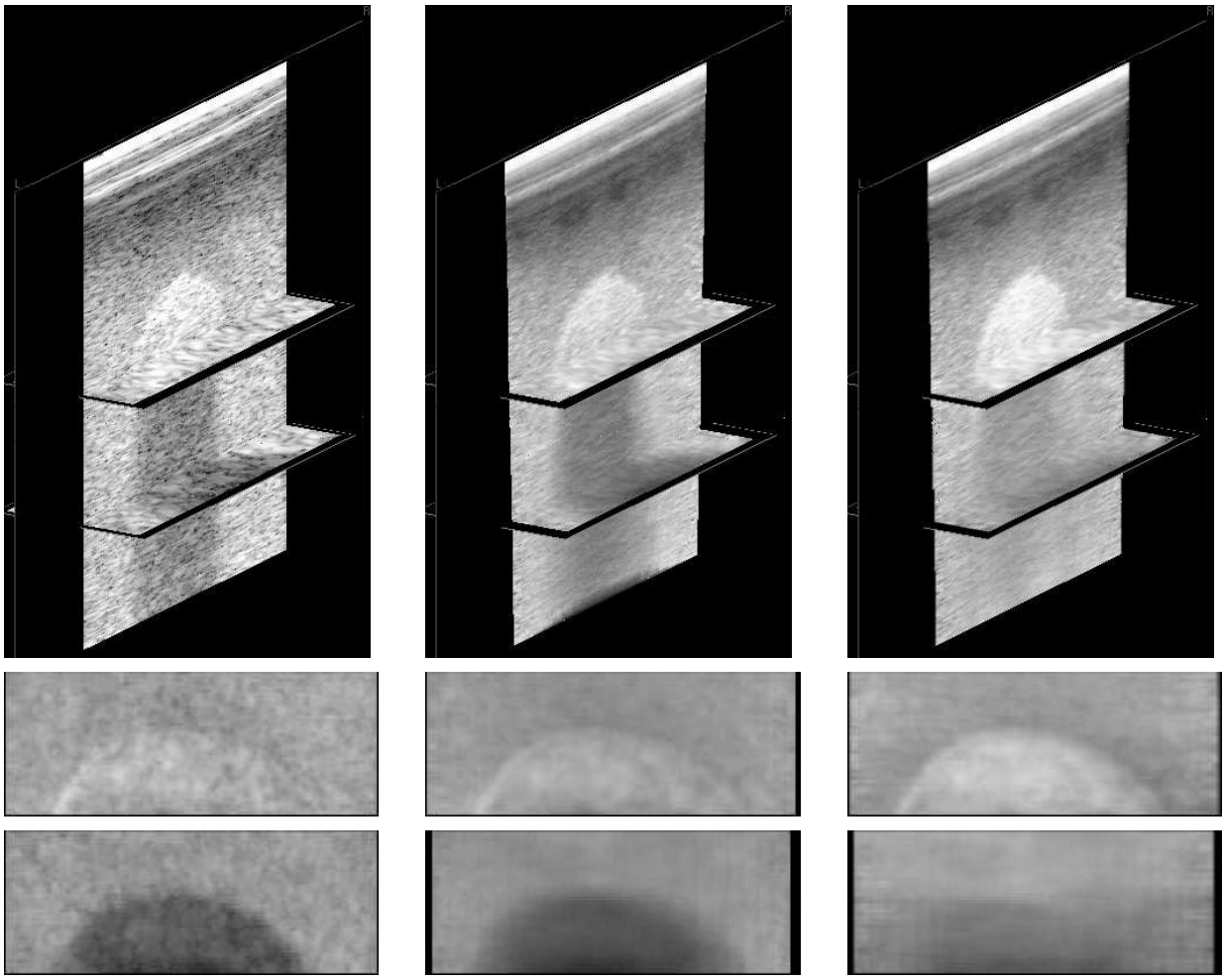

(a) BSCAN (b) COMPOUNDED (c) PAIRED

Figure 6: **3D scan of the olive phantom.** (a) Shows two orthogonal slices through a volume data set acquired with a linear volume probe. The lower rows show two C-scans (parallel to the phantom surface): one through the olive and one through the gelatin below the olive. (b) The same visualisations using conventional angular compounding. (c) Using the PAIRED algorithm — the contrast of the olive is increased, and that of the shadow reduced.

4 Discussion

It is clear from these results that, although most of the algorithms perform well on some data, PAIRED is the most consistent. Although there are many assumptions behind this algorithm, they are in fact less strong than those behind the alternatives. For instance, PAIRED *does* require isotropic scattering, however, SPEC_DIV and CENTRE_FREQ require scattering of exactly the same type as in the calibration phantom, i.e. both isotropic and with the same frequency distribution. In this regard, SCATTER is the most flexible, however unlike the other algorithms it suffers from the additional assumption that attenuation is proportional to backscatter.

This can be seen clearly in the results for the attenuation phantom, Table 4. It has already been noted that the distribution of scatterer size in the -17 dB spheres was not the same as in the other spheres or the phantom background. It is notable that, particularly for the SCATTER and CENTRE_FREQ methods, very different results are shown for these spheres compared to the others. PAIRED, on the other hand, shows consistent results for all spheres, since they all exhibit isotropic scattering, even if the backscatter spectrum is not the same in all cases.

It should be noted that none of the algorithms give particularly good resolution estimates of attenuation: all require significant filtering in order to provide sufficiently smooth estimates of cumulative attenuation c_{comp}, eq. (8) to preserve the appearance of the compounded images. In this regard, SCATTER is perhaps slightly better, with CENTRE_FREQ and PAIRED having the lowest resolution. Attenuation corrections are possible for the 0.5 cm spheres in Figure 4, however we would not expect to be able to resolve attenuation differences at a much smaller level than this.

It can be seen from Table 1 that the PAIRED algorithm is nearly as fast to execute as conventional compounding. Both SCATTER and PAIRED only require envelope data at relatively low resolution (i.e. a B-scan pixel size will suffice in both cases), whereas CENTRE_FREQ and SPEC_DIV require RF ultrasound data. Hence PAIRED is both faster and more convenient to implement than the alternatives.

Finally, the 3D data in Figure 6 demonstrates that our choice of the unknown variable $K(y)$ is not ideal for this scanning scenario. Recall that we set this such that the overall gain in any row of the compounded image is the same before and after attenuation correction. This is appropriate in individual images, since the time-gain control can be used to compensate for any unwanted vertical gain variation. For 3D data, however, we would like to have a normalisation which is consistent *across* scans. The current normalisation results in banding of C-scan re-slices through the data. This is particularly apparent in the lower images of Figure 6(c) — here the horizontal gain variation has been corrected, but this has resulted in an incorrect vertical gain variation.

5 Conclusions

We have shown that it is possible, at least on simulated and *in vitro* data, to estimate variations in lateral attenuation using scans from equal and opposite steered angles. These can be used to generate spatially compounded images with significantly reduced shadowing and enhancement artefacts. The algorithm performs as well as the best alternatives, and is more consistent over a range of data. Furthermore, it is relatively easy to implement and executes in real time.

There are a variety of possibly avenues for reducing the number of assumptions behind this algorithm. Firstly, we may be able to use the various steered scans to estimate (and correct for) the speed of sound before running the PAIRED algorithm. There have already been attempts to correct for speed of sound in angular-compounded images, either by modelling the sample as layered (Krucker

et al., 2004), or performing a non-rigid warping using radial basis functions (Groves and Rohling, 2004). Secondly, it may be possible to detect where we have directional rather than isotropic scattering, following on from the work of Wilhjelm et al. (2001), and adjust for this directionality.

Acknowledgements

Graham Treece is supported by an EPSRC/RAEng Postdoctoral Fellowship. Dynamic Imaging Ltd. provided a modified ultrasound machine with low-level access to the control software. This enabled the acquisition of analogue RF and digital amplitude ultrasound data in real time, and adjustments to the focusing required for beam steering.

References

Berson, M., Roncin, A., Pourcelot, L., 1981. Compound scanning with an electronically steered beam. Ultrasonic Imaging 3, 303–308.

Bevan, P. D., Sherar, M. D., 2001. B-scan ultrasound imaging of thermal coagulation in bovine liver: frequency shift attenuation mapping. Ultrasound in Medicine and Biology 27 (6), 809–817.

Entrekin, R., Jackson, P., Jago, J. R., Porter, B. A., Sep. 1999. Real time spatial compound imaging in breast ultrasound: technology and early clinical experience. MedicaMundi 43 (3), 35–43.

Entrekin, R. R., Porter, B. A., Sillesen, H. H., Wong, A. D., Cooperberg, P. L., Feb. 2001. Real-time spatial compound imaging: application to breast, vascular and musculoskeletal ultrasound. Seminars in Ultrasound CT and MR 22 (1), 50–64.

Flax, S. W., Pelc, N. J., Glover, G. H., Gutmann, F. D., McLachlan, M., 1983. Spectral characterization and attenuation measurements in ultrasound. Ultrasonic Imaging 5 (2), 95–116.

Frigo, M., Johnson, S. G., 1998. FFTW: An adaptive software architecture for the FFT. In: Proc. 1998 IEEE Intl. Conf. Acoustics Speech and Signal Processing. Vol. 3. IEEE, pp. 1381–1384.

Groves, A. R., Rohling, R. N., 2004. Two-dimensional spatial compounding with warping. Ultrasound in Medicine and Biology 30 (7), 929–942.

Hughes, D. I., Duck, F. A., 1997. Automatic attenuation compensation for ultrasonic imaging. Ultrasound in Medicine and Biology 23 (5), 651–664.

J. M. Kofler, J., Madsen, E. L., 2001. Improved method for determining resolution zones in ultrasound phantoms with spherical simulated lesions. Ultrasound in Medicine and Biology 27 (12), 1667–1676.

Jensen, J. A., 1996. Field: A program for simulating ultrasound systems. Medical and Biological Engineering and Computing 34, Supp. 1 (1), 351–353.

Jesperson, S. K., Wilhjelm, J. E., Sillesen, H., Apr. 1998. Multi-angle compound imaging. Ultrasonic Imaging 20 (2), 81–102.

Knipp, B. S., Zagzebski, J. A., Wilson, T. A., Dong, F., Madsen, E. L., 1997. Attenuation and backscatter estimation using video signal analysis applied to B-mode images. Ultrasonic Imaging 19 (3), 221–233.

Krucker, J. F., Fowlkes, J. B., Carson, P. L., Sep. 2004. Sound speed estimation using automatic ultrasound image registration. IEEE Transactions on Ultrasonics, Ferroelectrics and Frequency Control 51 (9), 1095–1106.

Pernot, M., Tanter, M., Bercoff, J., Waters, K. R., Fink, M., May 2004. Temperature estimation using ultrasonic spatial compound imaging. IEEE Transactions on Ultrasonics, Ferroelectrics and Frequency Control 51 (5), 606–615.

Rao, M., Chen, Q., Shi, H., Varghese, T., Mar. 2006. Spatial-angular compounding for elastography using beam steering on linear array transducers. Medical Physics 33 (3), 618–626.

Treece, G. M., Prager, R. W., Gee, A. H., Dec. 2005. Ultrasound attenuation measurement in the presence of scatterer variation for reduction of shadowing and enhancement. IEEE Transactions on Ultrasonics, Ferroelectrics and Frequency Control 52 (12), 2346–2360.

Tu, H., Varghese, T., Madsen, E. L., Chen, Q., Zagzebski, J. A., 2003. Ultrasound attenuation imaging using compound acquisition and processing. Ultrasonic Imaging 25 (4), 245–261.

Tu, H., Zagzebski, J. A., Gerig, A. L., Chen, Q., Madsen, E. L., Hall, T. J., May 2005. Optimization of angular and frequency compounding in ultrasonic attenuation estimations. Journal of the Acoustical Society of America 117 (5), 3307–3318.

Tyréus, P. D., Diederich, C., 2004. Two-dimensional acoustic attenuation mapping of high-temperature interstitial ultrasound lesions. Physics in Medicine and Biology 49 (4), 533–546.

Wilhjelm, J. E., Jensen, M. S., Jespersen, S. K., Falk, E., Feb. 2004. Visual and quantitative evaluation of selected image combination schemes in ultrasound spatial compound scanning. IEEE Transactions on Medical Imaging 23 (2), 181–190.

Wilhjelm, J. E., Pedersen, P. C., Jacobsen, S. M., Mar. 2001. The influence of roughness, angle, range and transducer type on the echo signal from planar interfaces. IEEE Transactions on Ultrasonics, Ferroelectrics and Frequency Control 48 (2), 511–521.

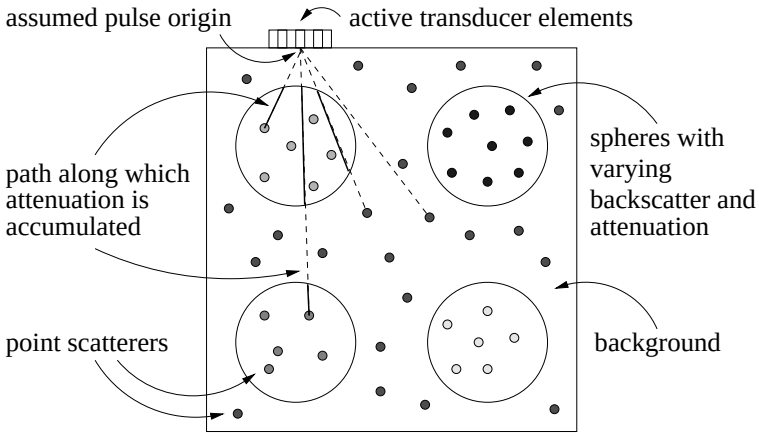

Figure 7: **Simulation of attenuation in Field II.** Although Field II can simulate varying backscatter and a uniform attenuation, it is not able to simulate a varying attenuation. A simulated phantom was constructed with four cylindrical inclusions each with varying backscatter and attenuation coefficients. 10^5 scatterers were distributed over the phantom, with backscatter magnitudes dependent on location within the phantom. At each location of the active transducer elements, the backscatter values for *all* scatterers were modified by the accumulated attenuation along a line between the scatterer and the assumed origin of the ultrasound pulse.

Appendix

A Simulation of attenuation in Field II

Field II does not have an inherent model for varying attenuation in a sample. This was modelled by modifying the backscatter for every point scatterer at every probe location, as explained in Figure 7. It should be noted that although this is a better simulation than simply varying the magnitude of the focused RF vector with depth, it does not model all the effects of attenuation on focusing. In addition, this model of attenuation does not take into account frequency shifts in the ultrasound pulse as it is attenuated. For this reason, it is not possible to use Field simulations created in this way to test the frequency-based methods of attenuation compensation, e.g. CENTRE_FREQ and SPEC_DIV.